

Figure 2. Photograph showing the Purisima Formation/terrace deposit contact along the backcliff portion of Seabright Beach (contact shown by arrow). Note the vegetated debris fan along the base. The geologic units shown here are nearly equal in thickness. However, to the west, the Purisima Formation (bottom) increases in proportion to terrace deposits (top), and to the east the Purisima Formation decreases until it is no longer exposed in outcrop on this side of the Santa

Cruz Harbor.



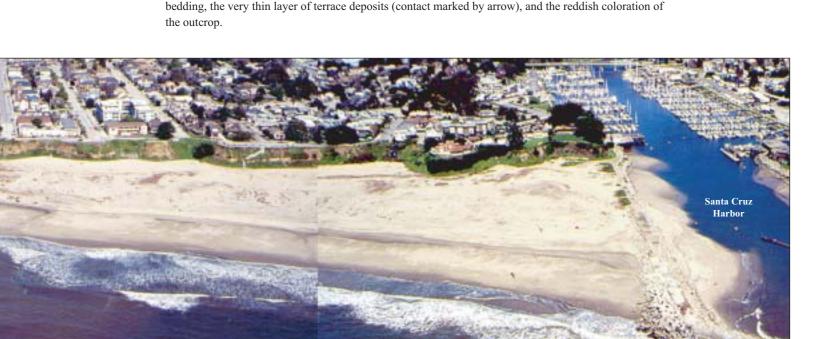


Figure 4. This oblique aerial photomosaic of Seabright Beach shows the layout of the beach with respect to San Lorenzo River and San Lorenzo Point to the west and the Santa Cruz Harbor Jetty to the east. The cliffs here range from 8 to 15 m and are highest near the Point. The accompanying equal-area stereonet plots of joints measured along the cliff face show a variation in joint orientations and joint sets along the back beach cliff and San Lorenzo point. The stereonet labeled A shows those joints mapped only along the north-south oriented San Lorenzo Point. In this representation, it can be seen that there are three primary joint sets. Two of these are near vertial and oriented NW and N-S; a nearly horizontal set strikes NNE. The stereonet labeled B shows those joints located along the 900-meter east-west stretch of cliff. The two primary joint sets measured along this section of cliff are oriented

INTRODUCTION The coastal cliffs along much of the central California coast are actively

episodic retreat threatens homes and community infrastructure. Research suggests that more along the adjacent 900-m, east-west oriented cliff section of Seabright Beach. erosion occurs along the California coast over a short time scale, during periods of severe Only one orientation of jointing (7°, near vertical) occurs in both the back-cliff storms or seismic activity, than occurs during decades of normal weather or seismic area and along the point. Along San Lorenzo Point on the western edge of Johnson, 1979 and 1983; Kuhn and Shepard, 1979).

an erosion hotspot (Moore and others, 1999; Griggs and Savoy, 1985). This map presents Where the joints are more regularly spaced, the cliff face takes on a point and flow may be focused. seacliff failure and retreat data from the Seabright Beach section, California, which is embayment morphology controlled by the jointing and blockfalls. Along the located on the east side of Santa Cruz (fig. 1) along the northern Monterey Bay coast. The eastern half of Seabright Beach, where the cliffs are composed primarily of data presented in this map series provide high-resolution spatial and temporal information terrace deposits, no distinct jointing was identified in the field. Overall the joints on the location, amount, and processes of seacliff retreat in Santa Cruz, California. These do appear to have some influence on the location and orientation of the seacliff data show the response of the seacliffs to both large magnitude earthquakes and severe failures, as the nearly conjugate joints along both the east-west section of cliff climatic events such as El Niños; this information may prove useful in predicting the future and San Lorenzo Point act as failure planes for blockfalls. response of the cliffs to events of similar magnitude. The map data can also be incorporated into Global Information System (GIS) for use by researchers and community Four sets of vertical aerial photographs (Oct. 18, 1989; Jan. 27, 1998; Feb. 9, (U.S. Army Corps of Engineers, 1985). Existing data from wave-gage records 1998; and March 6, 1998) were orthorectified and digital terrain models (DTMs) were and wave hindcasts show that deep water waves have a mean height of 1.2 m and

generated and edited for this study (see Hapke and Richmond, 2000, for description of a mean period of 13 seconds. The waves most frequently arrive from the seacliffs to seismic shaking, as well as to establish an initial cliff-edge position to measure than during non-El Niño winters, and heights of three meters or greater are the amount of retreat of the cliff edge over the following decade. The remaining three sets common. Wave refraction studies (U.S. Army Corps of Engineers, 1985) show of photographs were collected using the U.S. Geological Survey Coastal Aerial Mapping that for the Seabright Beach section of northern Monterey Bay waves System (CAMS) during the 1997-98 El Niño (see Hapke and Richmond, 1999; 2000). The approaching from the northwest diverge significantly around Point Santa Cruz at CAMS photographs were taken before, during, and after severe storms and are used to the northwestern entrance to the Monterey Bay, changing nearly 100° to examine seacliff response to these storms. In addition to the analyses of photogrammetrically processed data, field mapping identified joints, faults, and lithologic energy) is thus reduced before reaching the shoreline. However, waves variations along this section of seacliff.

The 0.9 km stretch of Seabright Beach extends from San Lorenzo Point on the reaching the shoreline in northern Monterey Bay are commonly storm waves west to the Santa Cruz Yacht Harbor on the east (figs. 1 and 2). The cliffs at Seabright approaching from the southwest to west. Beach are completely protected from wave attack by a wide beach. The protective beach is a relatively recent feature that formed after the emplacement of the Santa Cruz Yacht highest high water is 2.4 m and the lowest low is -0.8 m (U.S. Army Corps of Harbor jetty in 1963-1964. Prior to the completion of the jetty, the cliffs at Seabright Beach Engineers, 1985). The highest monthly tides occur in the winter and summer; it were subject to daily wave attack. The data in this study are post-jetty construction; therefore, the seacliff failures and cliff retreat are the result of nonmarine processes (rainfall, groundwater and seismic shaking).

The 8 to 15 m high cliffs at Seabright Beach are composed of the Miocene to annual precipitation since 1895 is 53 cm, although large climatic perturbations Pliocene Purisima Formation, which is overlain by unconsolidated Pleistocene terrace such as El Niño can bring excessive precipitation to the area. Based on data deposits (fig. 3) (Dupre, 1975; Greene, 1977; Brabb, 1989). The relative thickness of these compiled by Storlazzi and Griggs (2000), 76 percent of historical storms that units varies along the length of the cliff. At the west end of Seabright Beach, including San caused significant coastal erosion or damage occurred during El Niño years. Lorenzo Point, nearly the entire cliff section is composed of Purisima Formation and is capped by less than 2 m of terrace deposits (fig. 4). In this exposure, the Purisima Formation is a moderately weathered, moderately indurated massive sandstone. The height of the cliffs and the thickness of the Purisima Formation decrease to the east. In the cliffs immediately adjacent to the harbor, the entire exposure is composed of terrace deposits. Toe-slope debris and wind-blown sand form a nearly continuous fan along the cliff base that obscure the lower portion of the cliff.

Within the exposed portions of the Purisima Formation, joints exhibit a wide array of orientations (fig. 2). Most are steeply dipping, with the exception

WAVE AND CLIMATIC SETTING

documented seacliff slope failures. Long-term average erosion rates calculated for this on the western edge of Seabright Beach. Stereonet plots of the joints are shown earthquake, a 7.1 magnitude earthquake that caused widespread damage to the area section of coast (Moore and others, 1999) do not provide the spatial or temporal data in two separate plots because of the scattered nature of the data. Figure 4a shows stretching from Santa Cruz to the San Francisco Bay. The epicenter of the earthquake was resolution necessary to identify the processes responsible for retreat of the seacliffs, where joints mapped along San Lorenzo Point, while figure 4b shows the joints mapped located in the Santa Cruz Mountains, approximately 9 km inland from the coast. Peak accelerations in the vicinity of the coastal cliffs were estimated to be on the order of 0.47 g to 0.64 g (horizontal) and 0.40 g to 0.66 g vertical (Sydnor and others, 1990). Extensive block and debris falls, induced by the seismic shaking, occurred along the seacliffs in the quiescence (Griggs and Scholar, 1998; Griggs, 1994; Plant and Griggs, 1990; Griggs and Seabright Beach, joints are regularly spaced and more closely spaced than along study area (Plant and Griggs, 1990; Sydnor and others, 1990). Plant and Griggs (1990) the back-cliff area (fig. 4). The joints along San Lorenzo Point are infilled with a describe the seacliff failures in detail; in addition to the slope failures, they also describe This is the third map in a series of maps prepared to document the processes of reddish-brown material (Fe?) that is only found in this area. Joints along the eastshort-term seacliff retreat through the identification of slope failure styles, spatial variability west section of Seabright Beach are irregularly spaced; in some areas the spacing be important in determining locations of failures in the days, weeks, and even years of failures, and temporal variation in retreat amounts in an area that has been identified as is 3 to 4 m and in other areas there is a gap of nearly 20 m where no joints occur. following the earthquake by providing failure planes and zones along which groundwater brought increased winter storm activity to the coastline of the northern Monterey Bay. Associated with these storms, which began in force in late January of 1998, were increased wave energy from more westerly directions than in non-El Niño years, elevated sea level, and increased amount and duration of precipitation. While increased wave energy and elevated sea level potentially have significant impacts on those portions of the cliffs that are exposed to waves, increased rainfall leading to excessive surface wash and increased

groundwater pore pressures promote erosion of the seacliffs. The wave climate is well documented for the northern Monterey Bay CLIFF RETREAT techniques). The earliest set of photography is from 1989, taken immediately following the northwest, but they do approach from due south through north-northwest. During October 1989 and from March 1998. Digitizing while viewing in stereo ensures that the Loma Prieta earthquake. These photographs are used to document the response of the El Niño winters, storm waves arrive more frequently from the west and southwest true topographic break in the terrain is used as the cliff edge. The cliff edge is typically approach the shore from the southwest. Wave height (and consequently wave approaching from the southwest undergo less refraction because there is no headland to dissipate wave energy. As a result, waves from the southwest have greater heights and more energy upon reaching the shoreline. The highest waves morphologic evolution of this stretch of coast from October 1989 to March 1998. The Tides in this region are diurnal and have a mean range of 1.6 m; the is not unusual for the highest tides to coincide with large, winter storm waves.

> Rainfall in this region occurs predominantly from December through March, and high rainfall frequently coincides with large waves. The average section, where the cliff retreated approximately 4.5 m. The amount that a particular section of cliff retreats in a given time period provides quantitative information that may be useful to land-use planning and land owners. While such retreat information is valuable, it provides little information on the processes of

> > slope failure that lead to seacliff retreat.

SEISMIC AND CLIMATIC EVENTS

This study documents the impacts of earthquakes and large storms to the The second major event considered in this study is the 1997-98 El Niño that

The amount of cliff retreat for the Seabright Beach section was determined by digitizing the top edge of the cliff on the rectified photographic stereo models from sharp and easy to identify, but in some areas it is completely obscured by large trees or other vegetation. The amount of landward retreat of the cliff edge was measured as the difference in distance between two cliff edges (as digitized on the October 1989 and March 1998 stereomodels) as measured from a shore parallel baseline. The use of shore parallel baselines in measuring coastal change is a common technique in coastal studies (Anders and Burns, 1991; Thieler and Danforth, 1994). For this map, the positional accuracy is less than 1 m, based on the scale of the photography, the scan resolution, and the global positioning system (GPS) survey data used in the orthorectification process. The orthophotomosaic in figure 5 shows the cumulative seacliff retreat and October 1989 data (orange line) shows the position of the upper cliff edge immediately following the magnitude 7.1 Loma Prieta earthquake, and the March 1998 data (green line) represents the position of the cliff edge following the last of the severe 1997-98 El Niño storms. The amount of retreat in the bar graph in figure 5 shows a maximum retreat of 5.8 m. The baseline from which the cliff edge positions are measured is parallel to the average trend of this section of cliffs. However, the cliff morphology is crenulated and as a result the distance along the baseline (fig. 5) is shorter than the actual distance along the cliff edge. The maximum retreat (5.8 m) is located at the west end of this section where there is now a retaining wall along the upper part of the cliff. The only other area that experienced any significant (greater than 2 m) retreat of the cliff edge is on the eastern part of the

Aerial photography from Coastal Aerial Mapping System (CAMS), February 9, 1998 Universal Transverse Mercator projection, zone 10 October 1989 - Winter 1998 — Winter 1998 - Februray 1998 — February 1998 - March 1998

Aerial photography from Coastal Aerial Mapping System (CAMS), February 9, 1998 Universal Transverse Mercator projection, zone 10 Figure 6a. Enlarged section of the western portion of orthophoto mosaic (fig. 5, A) showing failure signatures for four time periods.

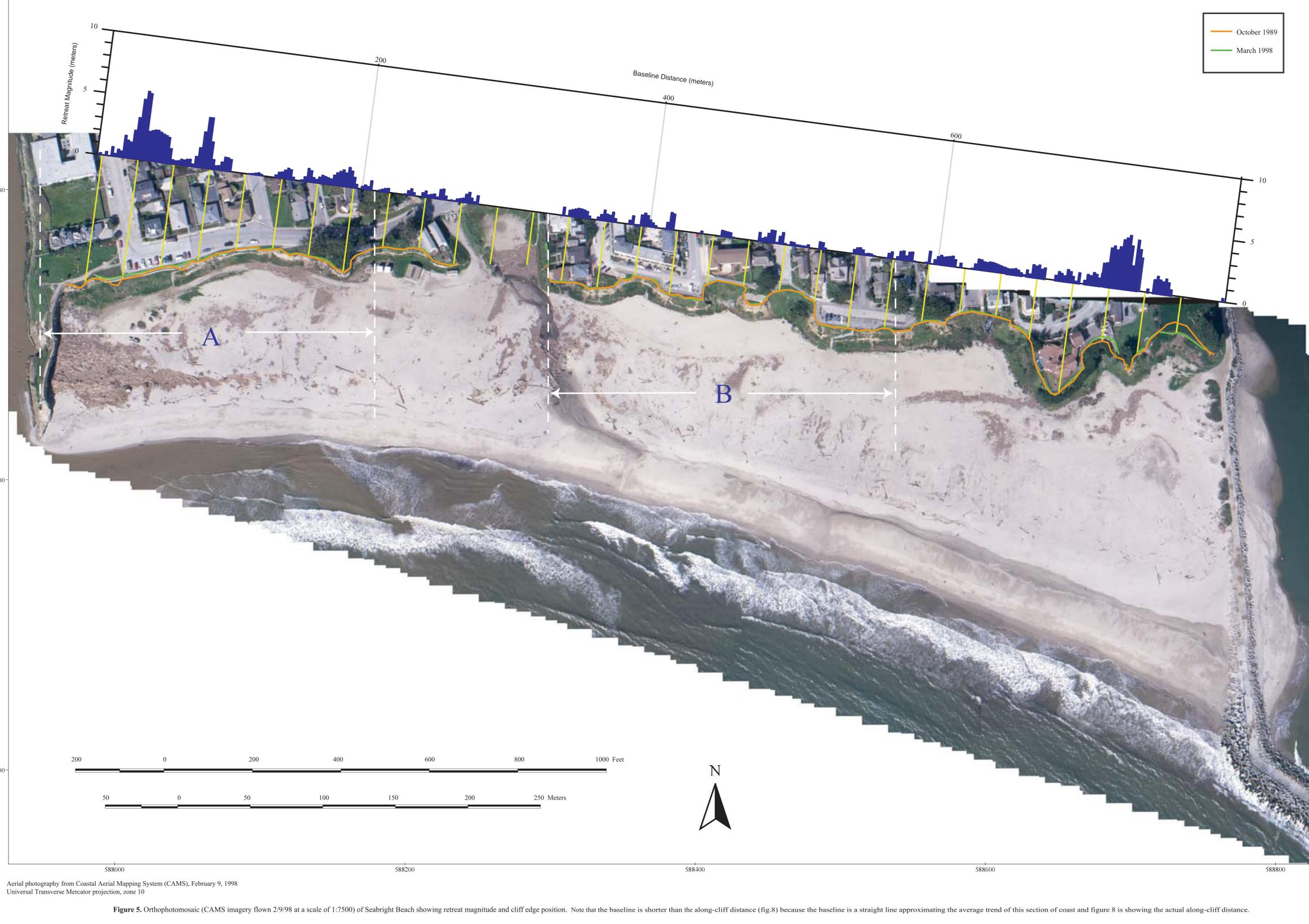




Figure 6b. Enlarged section of the eastern portion of orthophotomosaic (fig. 5, B) showing failure signatures for four time periods.

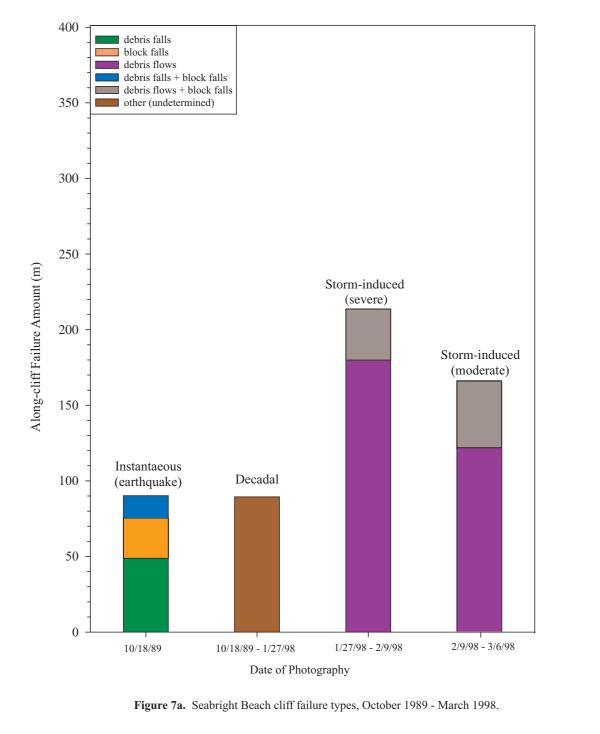
Aerial photography from Coastal Aerial Mapping System (CAMS), February 9, 1998

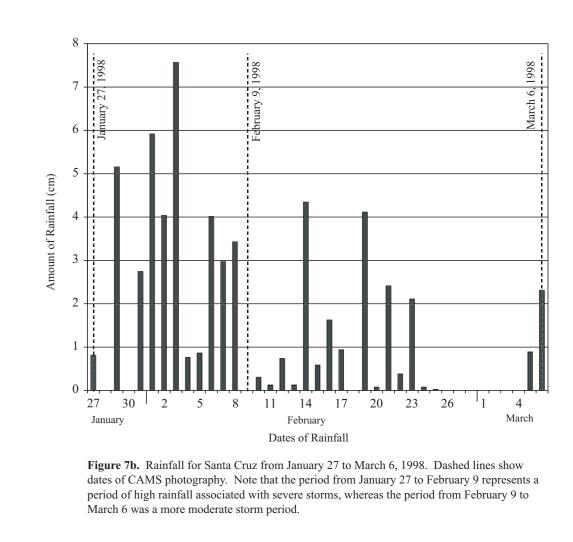
Universal Transverse Mercator projection, zone 10

Table 1. Linear extent of cliff section experiencing slope failure for each of the time periods investigated. The data is further subdivided to show the type of slope failure for each occurrence, as well as the geologic units involved, if distinguishable.

Time Interval	Debris falls (m)	Block falls (m)	Debris flows (m)	Mixed fall block and debris (m)	Block fall and debris flow (m)	Other (m)	Total along-cliff failure per interval
0 (instantaneous)	48.8 Qmt**	26.7 Tp**	0	14.8 Qmt and Tp**	0	0	90.3
8.27 yrs (Oct. 89 – Jan. 98)	0	0	0	0	0	89.4	89.4
0.03 yrs (Jan. 98 – Feb. 98)	0	0	179.9 Qmt**	0	33.8 Qmt and Tp**	0	213.7
0.07 yrs (Feb. 98 – March 98)	0	0	121.1 Qmt**	0	44.0 Qmt and Tp**	0	165.1
Total along-cliff failure per failure type	48.8	26.7	301.0	14.8	77.8	89.4	

* Other, failures where type of failure could not be determined ** Qmt, terrace deposit; Tp, Purisima Formation





Types of cliff failures Tp failures △ January 1998 to February 1998 — Mixed failures February 1998 to March 1998

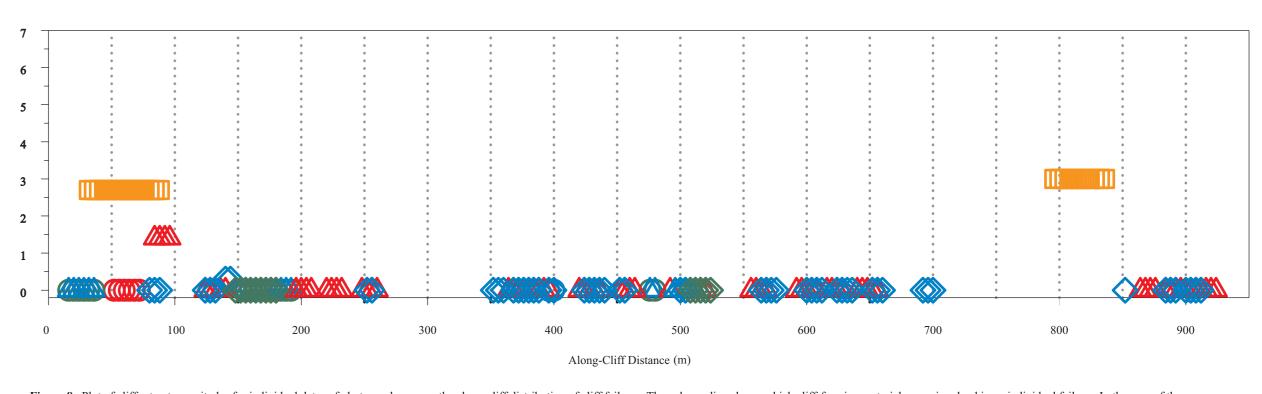


Figure 8. Plot of cliff retreat magnitudes for individual dates of photography versus the along-cliff distribution of cliff failures. The color coding shows which cliff-forming materials were involved in an individual failure. In the case of the area near the beginning of the section (between 0 m and 50 m), cliff failure was identifed in the October 1989 photography as failure involving a mixture of the Purisima Formation and the terrace deposits. This is represented by the green circles. Note that all "retreat" values for the October 1989 date of photography are shown as zero. This date was used as the baseline data, and thus no other data set currently exists against which to determine the amount of retreat for this date. However, along-cliff failures are identified by deposits on the beach and scars on the cliff slope. The along-cliff distance is longer than the baseline shown in figure 5 because the baseline is a straight line approximating the average trend of this section of coast and figure 8 is showing the actual along-cliff distance.

PROCESSES OF SEACLIFF FAILURE During this study we developed a method for investigating shortterm processes of seacliff evolution using rectified photographic stereo models. This method allows us to document the linear extent of cliff failures, ne spatial and temporal relationship between failures, and the type or style of In order to document the along-cliff linear extent of slope failure associated with a particular period or event, the top edge of the cliff was digitized from the rectified photographic stereo model at high resolution (0.2 m/pixel) for each date of photography. At each location where slope failure was observed, either by retreat of the cliff edge or by visible deposits at the base of the cliff, the position, linear extent, and characteristics of the cliff failure were documented. The characteristics for each occurrence of slope failure include the amount of retreat, if any, the type of failure (debris fall,

(linear or cuspate), and the geologic unit involved. The type of cliff failure was determined by both the nature of the failure scar and the deposit on the beach below and is based on the classifications and descriptions by Varnes (1958). The linear extent of places where the cliff has failed is demarcated for each date of photography by overlaying the representation of the cliff edge that was digitized from the previous date of photography on the current rectified photographic stereo model (for example Oct. 1989 digitized cliff edge positioned over Jan. 1998 stereo model) and delineating the places where visible slope failure or retreat of the top edge of the cliff have occurred during the period between the two dates of photography. For each linear extent of slope failure the location and characteristics of each individual failure for each date are recorded. An important finding of this study is that slope failures do not always result in retreat of the cliff edge. Failures can occur on the seaward face of the cliff where there is no actual landward retreat of the top edge of the cliff. These slope failures are recognized by the existence of fresh scars and deposits that are visible in the photographic stereo models. The cliff failures that do not result in measurable retreat of the top edge of the cliff may result in destabilization of the cliff and are important in the understanding of seacliff evolution and processes. Along Seabright Beach, slope failures were documented along nearly the entire cliff section, although significant (> 1 m) retreat of the cliff edge occurred in only two locations, near the east and west ends of the section. These two locations are shown as areas A and B on figure 5. Figure 6a shows cliff failures along an enlargement of the western area A. In this area, failures occurred nearly continuously along 200 m of cliff and were recorded during all time periods of the study (colored lines). Within area A failures occurred in the same place as or immediately adjacent to locations of

previous failures. Figure 6a shows that a 75 m length of cliff failed during the decade from 1989 to 1998 (red line). A retaining wall was built in this location and has impeded the retreat of the cliff since its construction. The cliff, as a result, did remain stable during the 1997-98 El Niño storms, although slope failures during these storms were documented slightly east of the retaining wall along a 55-m-long section (fig. 6a, blue and green lines). Another area of cliff failure is shown in figure 6b, an enlargement of area B in figure 5. The cliffs in this area failed in a similar manner during the Loma Prieta earthquake and the 1997-98 El Niño. There was no significant retreat (< 1 m) documented during any specific time interval. Recent scars and deposits identified from the rectified photographic stereo models show that the linear geomorphic expression of each individual failure is small (4 to 10 m) even though the cliff did fail along much of the length shown in figure 6b. Failures commonly occur on the face of the cliff, undercutting the asphalt of overlying roads and parking lots, but result in no measurable retreat of the top edge of the cliff. In general, the overall distribution of seacliff failures along the Seabright Beach section reveals widespread slope failure characterized by many small linear failures on the slope face. A more continuous style of failure occurs in the west half of the cliff section where the majority of the cliff is composed of the Purisima Formation. The smaller failures occur primarily where the cliff is predominantly composed of terrace deposits.

Figures 7 and 8 and table 1 summarize the overall failure styles, retreat amounts, slope failure distribution, and rainfall amounts along Seabright Beach. In figure 7a, the failure types are shown in relation to the time of occurrence and the amount of the section that failed, and Table 1 shows the total amount of cliff failure for each time interval as well as the

failure types. Table 1 also includes the geologic unit that failed, if this was distinguishable on the aerial photography. The category labeled "other" represents decadal slope failures wherein cliff retreat was documented but the failure style could not be discerned. Three different types of slope failure were documented during the period from October 18, 1989 to March 6, 1998. These include debris falls, block falls, and debris flows. Rapid, seismically induced failures were either Survey Open File Report 77-718, 347 pp. block or debris falls, resulting in failure of 90 m of the 0.9 km-long cliff Griggs, G.B., and Johnson, R.E., 1979, Coastal Erosion, Santa Cruz result of seismic shaking may have contributed to the failure of the cliffs in the decade since the Loma Prieta earthquake, in which 89 m of the cliff experienced some failure and resulted in significant retreat of the cliff edge in two locations. In some areas, the process of failure could not be identified due to lack of a geomorphic scar or a characteristic toe deposit. These areas were identified by a retreat of the cliff edge and are included as "other" in table 1, whereby the cliff retreated but the process was not interpretable. The 89 m of decadal failures were all included in this "other" category. The dominant failure type documented from the February 1998 imagery is debris flows of the terrace deposits. The period of severe storms in the several weeks prior to February 9, 1998, had the greatest impact on this stretch of coast. Over 213 m of the cliff failed during this period, predominantly by the process of debris flows involving the terrace deposits. During the last several weeks of the El Niño storm period, precipitation amounts dropped and storm intensities decreased (fig 7b). The response of the seacliffs during this time was still significant; failures were documented along 165 m of the section. Debris flows and minor block falls were the two types of failures identified during this period. Figure 8 is a plot of the distribution and amount of cliff failure

along Seabright Beach. The along-cliff distance in figure 8 is longer than the baseline shown in figure 5 because the baseline is a straight line approximating the average trend of this section of coast and figure 8 is showing the actual along-cliff distance. All failures documented from October 1989 are shown as having zero retreat amounts. The amount of landward retreat of the cliff edge is not shown for the October 1989 date in figure 8 because the cliff position delineated from this date of photography was used as the initial position against which to measure subsequent retreat. Failure types can be recognized by geomorphic scars or toe deposits, but retreat amounts cannot be documented. Figure 8 demonstrates the nearly continuous occurrence of failures with a small amount of retreat occurring at two distinct locations. The area that was retreating in the western portion has now been stabilized with a retaining wall and consequently did not fail during the 1997-98 El Niño. The amounts of retreat on figure 8 are for each individual time period, whereas those shown on the bar graph on figure 7a are cumulative. The amount of failure of the terrace deposits (blue on fig. 8) is much more widespread than those within the Purisima Formation (red), and most of the documented slope failures resulted in no measurable retreat of the cliff edge. However, the pervasiveness of the slope-face failures causes a steepening of the cliff face which may result in a less stable slope prone to future failures. This map has introduced new techniques of analyzing the shortterm evolution of seacliffs and the differential response of seacliffs to seismic and climatic events. Using stereo models derived from softcopy photogrammetry, we are able to locate seacliff failures to determine their spatial distribution and the geologic units involved for several different time periods in an area where seacliff failure and retreat periodically threaten homes and community infrastructures. These data can be incorporated into a GIS database to examine the relationship of the failures to one another, to coastline morphology, and to field data (faults, joints, or lithologic changes). Spatial plots of the failures appear to show specific patterns; if additional data continue to support this observation, the technique of analyzing the temporal and spatial distributions of the cliff failures outlined in this study may help to identify areas prone to future failures.

Anders, F.J., and Byrnes, M.R., 1991, Accuracy of shoreline change rates as determined from maps and aerial photographs: Shore and Beach, v. Brabb, E.E., 1989, Geologic map of Santa Cruz County, California: U.S. Geological Survey Miscellaneous Investigation Series Map I-1905, scale Dupre, W.R., 1975, Maps showing geology and liquefaction potential of Quaternary deposits in Santa Cruz County, California, U.S.: U.S. GeologicalSurvey Miscellaneous Field Studies Map MF-648, scale Greene, H.G., 1977, Geology of the Monterey Bay region: U.S. Geological Griggs, G.B., and Johnson, R.E., 1983, Impact of 1983 Storms on the coastline of Northern Monterey Bay, Santa Cruz County: California Geology, v. 36, no. 8, p.163-174. Griggs, G.B., and Savoy, L., eds., 1985, Living with the California coast: Durham, North Carolina, Duke University Press, 393 p. Griggs, G.B., 1994, California's Coastal Hazards: Journal of Coastal ResearchSpecial Issue No. 12, p.1-15. Griggs, G.B, and Scholar, D.C., 1998, Coastal erosion caused by earthquake- induced slope failures: Shore and Beach, v. 65, no. 4, p. 2-7. Hapke, C.J., and Richmond, B.M., 2000, Monitoring beach morphology changes using small-format aerial photography and digital softcopy photogrammetry: Environmental Geosciences Special Issue on Coastal Hazard Mapping Techniques, v. 7, no. 1, p. 32-37. Hapke, C.J., and Richmond, B.M., 1999, The development of a coastal aerial mapping system (CAMS) and its application to the study of coastal morphodynamics: Coastal Sediments '99, v. 3, p. 2398-2413. Kuhn, G.G., and Shepard, F.P., 1979, Accelerated beach-cliff erosion related to unusual storms in southern California: California Geology, v. 32, no. 3, p. 58-59. Maher, Norman, and Wong, F.L., 2001, Low-resolution (250-m) gridded bathymetry and shaded relief image (CCALBATG, CCALSHD.TIF) of the region offshore of central California between Point Reyes and San Simeon, in Wong, F.L., and Eittreim, S.E., Continental Shelf GIS for the Monterey Bay National Marine Sanctuary: U.S. Geological Survey Open-File Report 01-179. Moore, L.J., Benumof, B.E., and Griggs, G.B, 1999, Coastal Erosion Hazards in Santa Cruz and San Diego Counties, California: Coastal Erosion Mapping and Management, Journal of Coastal Research Special Issue No. 28, p. 121-139. Plant, N.G., and Griggs, G.B., 1990, Coastal landslides caused by the October 17,1989 earthquake, Santa Cruz County, California: California Geology, v. 43, no. 3, p.75-84. Storlazzi, C., and Griggs, G.B., 2000, The influence of El Niño-Southern Oscillation (ENSO) events on the evolution of central California's shoreline: Geological Society of America Bulletin, v. 112, no. 2, p. 236-Sydnor, R.H., Griggs, G.B., Weber, G.E., McCarthy, R.J., and Plant, N.G., 1990, Coastal bluff landslides in Santa Cruz County resulting from the Loma Prieta earthquake of 17 October, 1989: The Loma Prieta (Santa Cruz Mountains, California) earthquake of 17 October 1989: California Department of Conservation, Division of Mines and Geology, Special Publication 104, p. 67-82. Thieler, E.R., and Danforth, W.W., 1994, Historical shoreline mapping

(II): Application of the digital shoreline mapping and analysis system

Coastal Research, v. 10, no. 3, p. 600-620. U.S. Army Corps of

California storm and tidal waves study, Ref. No. CCSTWS 85-2.

Varnes, D.J., 1958, Landslide types and processes: Highway Research

Engineers, 1985, Geologic framework report, Monterey Bay, coast of

(DSMS/DSAS) to shoreline change mapping in Puerto Rico: Journal of

Any use of trade, firm, or product names in this publication is for descriptive purposes only and does not imply endorsement

Board Special Report 29, p. 20-27.